NASA TECHNICAL MEMORANDUM

NASA TM X-73494

NASA TM X-73494

CYCLIC STRUCTURAL ANALYSIS OF AIR-COOLED GAS TURBINE BLADES AND VANES

by Albert Kaufman and Raymond E. Gaugler
Lewis Research Center
Cleveland, Ohio 44135

TECHNICAL PAPER to be presented at the
Aerospace Engineering Conference sponsored by the
Society of Automotive Engineers
San Diego, California, November 29-December 2, 1976

CYCLIC STRUCTURAL ANALYSES OF AIR-COOLED GAS TURBINE BLADES AND VANES

by Albert Kaufman and Raymond E. Gaugler
NASA Lewis Research Center
Cleveland, Ohio 44135

E-8892

ABSTRACT

The creep-fatigue behavior of a fully impingement-cooled blade for four cyclic cases was analyzed by using the Elas 55, finite-element, nonlinear structural computer program. Expected cyclic lives were calculated by using the method of Strainrange Partitioning for reversed inelastic strains and time fractions for ratcheted tensile creep strains. Strainrange Partitioning was also applied to previous results from a one-dimensional cyclic analysis of a film-impingement-cooled vane. The analyses indicated that Strainrange Partitioning is more applicable to a constrained airfoil such as the film-impingement-cooled vane than to the relatively unconstrained fully impingement-cooled airfoil.

STAR category 39

INELASTIC STRAINS can be induced in airfoils as a result of high thermal stresses during engine transients and creep during steady-state operation. Repetition of inelastic straining under normal engine operation results in progressive creep-fatigue damage and eventual failure by cracking. A major difficulty in applying cyclic life prediction methods such as Strainrange Partitioning (1 to 3)* to a turbine blade is that the computation of inelastic strain cycles is a formidable undertaking.

In advanced aircraft engines, the high-pressure-stage turbine blades and vanes involve geometries and environments that require the use of three-dimensional, finite-element, stress analysis programs. Nonlinear, structural analysis computer programs are necessarily complex and, for large problems, use substantial amounts of computer time and storage.

One-dimensional stress analyses based on strength-of-materials theory have been extensively used in the design and cyclic analyses of cooled turbine blades because of their relative simplicity and because nonlinear three-dimensional structural programs have not been available until recent years. The one-dimensional analyses were adequate, provided the section analyzed was a chord width away from the end and the spanwise metal temperature gradients were reasonably linear. In (4) and (5), strain hysteresis loops were computed from one-dimensional programs for air-cooled vanes and blades with airfoil aspect ratios of approximately 2. However, a one-dimensional stress analysis would be of questionable validity for cooled blades having aspect ratios of the order of 1 and nonlinear spanwise temperature gradients, as is discussed in (6).

Strainrange Partitioning, which has been developed at the NASA Lewis Research Center by Manson, Halford, and Hirschberg, is a method for calculating low-cycle fatigue life under conditions of complete inelastic strain reversal. The inelastic strain hysteresis loops are divided into four basis components:

(1) Tensile plastic strain reversed by compressive plastic strain, $\Delta\epsilon_{pp}$

(2) Tensile plastic strain reversed by compressive creep strain, $\Delta\epsilon_{pc}$

(3) Tensile creep strain reversed by compressive plastic strain, $\Delta\epsilon_{cp}$

Kaufman

*Numbers in parenthesis designate References at the end of paper.

(4) Tensile creep strain reversed by compressive creep strain, $\Delta\epsilon_{cc}$

In cases where complete inelastic strain reversal does not take place, additional consideration must be given to the unreversed component of strain through a ductility exhaustion or time fractions approach.

The purposes of this study were, first, to demonstrate the use of an advanced, nonlinear, stress analysis computer program in calculating blade life and, second, to evaluate the effects of airfoil thermal and mechanical loading conditions and geometry on the inelastic strain cycles and the general applicability of the Strainrange Partitioning method. It is not the intention of this paper to verify the accuracy of the Strainrange Partitioning method since this is beyond the limited experimental information available and the accuracy of some of the analytical results.

An impingement-cooled blade was analyzed for an assumed cycle between effective gas temperatures at midspan of 1089 K (1599° F) to 1839 K (2850° F) with a coolant temperature of 533 K (500° F). The cycle consisted of acceleration and deceleration transients of 4 seconds each and a 30-minute hold time at the high-temperature part of the cycle. Transient metal temperatures were computed from a quasi-three-dimensional heat transfer analysis program. The thermal transients and chordwise temperature gradients were subsequently altered to increase the severity of the thermal loading, and the mechanical loads were removed to simulate a vane problem. Inelastic strains were computed from a three-dimensional, finite-element computer program for the solution of nonlinear problems involving creep and plasticity (7) and (8). Cyclic life was calculated from Strainrange Partitioning relations for the reversed portion of the strain cycle and by time fractions for the unreversed steady-state creep portion. In all, the design case and three parametric cases were analysed for the impingement-cooled blade configuration.

Strainrange Partitioning was also applied to the inelastic strain hysteresis loops computed for the design case of a film-impingement-cooled vane in (4) by a one-dimensional stress analysis program. The predicted lives at critical locations of this vane were compared with experimental results from cyclic tests in a static cascade facility at the NASA Lewis Research Center reported in (4).

ANALYTICAL PROCEDURE

The heat transfer, stress analysis, and life prediction methods used for the impingement-cooled blade study are described. The strain hysteresis loops for the film-impingement-cooled vane were computed by using experimental and calculated transient temperatures and a one-dimensional cyclic stress analysis program based on a kinematic hardening rule. These are described in (4) and will not be further discussed herein.

TRANSIENT TEMPERATURE ANALYSIS - A quasi-three-dimensional, time-dependent, thermal analysis computer program (9) was used to calculate the transient temperature distribution for the cyclic stress-strain analysis. The program computes the temperature and coolant flow distribution for a turbine blade cooled by impingement and crossflow convection.

The blade selected for this analysis was a cast shell airfoil with an impingement insert. Fig. 1 shows a schematic cross-sectional view of the blade. Chord length and blade span are both 3.8 cm (1.5 in.), and the wall thickness is tapered from 0.127 cm (0.050 in.) at the hub to 0.076 cm (0.030 in.) at the tip. The impingement insert is also tapered to maintain a uniform coolant-channel width. The forward region of the blade is cooled by impingement, and the spent impingement air flows chordwise through the trailing edge, cooling that region by forced convection.

Input to the program includes a description of the geometry, an estimate of total coolant flow, the coolant supply pressure and temperature at the hub end of the insert, the hot-gas-side heat transfer coefficient distribution, the gas total temperature distribution, and the gas static pressure at the trailing edge. For a transient calculation, tables of coolant supply pressure, hot-gas temperatures, hot-gas static pressure at the trailing edge, and wheel speed as a function of time are required.

The blade to be analyzed was divided into radial sections by chordwise planes and the layers were treated individually, except that thermal communication between sections was maintained in the three-dimensional heat conduction equations. The coolant-channel flow for each layer was treated as one-dimensional compressible flow with friction, heat transfer, and mass addition. Fig. 1 shows how a layer is divided into calculation stations and the arrangement

of nodes at a station.

The calculational procedure requires that an initial steady-state solution be determined. The calculations begin at the hub end of the blade and are marched radially through the blade, layer by layer. At each layer, the mean pressure and temperature in the coolant insert is calculated, assuming adiabatic flow with friction. These conditions are then used, along with the latest coolant-channel pressure distribution, to calculate the impingement jet flows and heat transfer coefficients. Using the new heat transfer data, the wall conduction finite difference equations and the coolant-channel energy equations are solved for a new temperature distribution, and the coolant-channel momentum equation is solved for a new pressure distribution. This is then used to recalculate impingement flows, and the calculations are repeated until four successive pressure distributions match within a specified tolerance band. This procedure is repeated for each layer of the blade. For the initial steady state, after all layers are complete, the total coolant used is compared with the initial estimate. If they do not match within tolerances, the inlet flow is adjusted and the calculations are repeated. Once the steady state has been established as an initial condition, the transient calculations are started. The program solves the transient finite difference equations for conduction in the blade wall and the time-dependent energy and momentum equations in the coolant channel.

STRESS ANALYSIS METHOD - Analyses were performed with a modified version of the Elas 55 computer program for the in-core solution of structural problems involving time-independent inelasticity and thermally activated, time-dependent inelasticity. The theoretical background and capabilities of this program are discussed in (7) and (8). The main plasticity and creep equations are described in the appendix. Elas 55 was extended to accommodate problems involving rotating machinery and reversed inelastic strain.

Plasticity computations are based on the von Mises yield condition and associated flow rule and assume isotropic hardening. The original version of Elas 55 used a viscoelastic Kelvin model to compute creep strains. However, this model was found to be inadequate to correlate the creep characteristics of the nickel-base superalloy blade material, cast IN 100.

To increase the accuracy of the creep computations, a secondary creep rate term was added to the creep equations and the Kelvin model was used essentially to calculate the primary creep strains.

To avoid introducing instabilities, the creep computations for steady-state hold times have to be performed in fine time increments. However, this incremental approach reduces the accuracy of the calculated creep strains because the correlated creep characteristics are being extrapolated to strain levels several magnitudes smaller than is warranted by the experimental data.

The analytical results were related to uniaxial stress-strain and creep data by combining the stress and strain components in terms of effective (von Mises) stresses and strains. Determining the signs of the effective plastic and creep strains presented a problem since both equations (A2) and (A12), in the appendix, always give positive values. Therefore, signs were allocated to the effective strain increments based on the signs of the normal stresses with the greatest magnitude during the time increment.

The program calculates average stresses and strains at the centroid of each element. Thermal load vectors were based on nodal point temperatures obtained from the heat transfer analysis.

STRESS-STRAIN DIAGRAM - The stress-strain curve for a virgin material during the first cycle is not representative of the stress strain behavior for subsequent cycles and may give rise to substantial errors if used for cyclic life prediction. Extensive cyclic tests of blade and vane materials have shown that, for a given strain range, the cyclic stress-strain hysteresis loop will attain a stable form after a relatively small number of cycles, as typified by the loops shown in Fig. 2.

Neither isotropic nor kinematic hardening specify this type of stress-strain behavior; in fact, neither of these hardening models will give a stable cyclic stress-strain diagram unless the strain hardening parts of the diagram are straight and parallel lines. The type of stress-strain response exhibited in Fig. 2 could be more accurately represented by Mroz or Kaufman mechanical sublayer models, as discussed in (10). The major drawback in using either the Mroz or mechanical sublayer models in large-scale problems such as cyclic loading of tur-

bine blades is that the storage requirements for these models are much greater than those for isotropic hardening. It is of interest that (10) also demonstrates that kinematic hardening can give less accurate results than isotropic hardening under multiaxial loading.

To represent the actual cyclic stress-strain diagram by an isotropic hardening model, a rectangular diagram with the same plastic strain range was assumed, as shown in Fig. 2. The yield strength was selected so that the plastic strain energies represented by the enclosed areas of the isotropic and actual stress-strain diagrams were kept approximately the same. The yield strengths are both temperature and strainrange dependent. Temperature dependence effects were obtained from cast IN 100 monotonic stress-strain curves presented in (11). Strainrange effects were determined from the results of cyclic stress-strain tests at 1200 K (1700° F) of cast IN 100 thin-wall tubular specimens performed at the Lewis Research Center by using the techniques described in (12). These data are plotted in Fig. 3 in terms of stress and plastic strain ranges with zero mean stresses and strains. The cyclic frequency was 0.5 Hz.

To apply the strainrange corrections, the problem had to be run first with estimated yield stresses to obtain a preliminary solution. The yield strengths at the elements that exhibited yielding were then corrected on the basis of Fig. 3 and the problem was rerun. Because of the computing time involved, it was not possible to carry this process through to a completely iterated solution. If the stresses at the most critical locations agreed reasonably well with the data of Fig. 3, the iteration was stopped at the second solution. In no case was the problem carried beyond a third iteration.

STRESS ANALYSIS PROCEDURE - The airfoil shell was modeled by using 165 eight-node hexahedral elements in five spanwise layers with a total of about 1200 unsuppressed degrees of freedom; the modeling around the airfoil cross-section is illustrated in Fig. 4. Blade taper and tilt were accounted for in determining the coordinates of the mesh network.

The load-time history was set up so that a cycle consisted of 24 increments of temperatures and mechanical loads; the latter included both centrifugal and gas pressure loading. A hold time of 30 minutes was applied at the high-gas-temperature part of the cycle. To obtain a sol-

ution for a cycle, the problem was run for an additional half cycle and the strain cycle or hysteresis loop used for life prediction was determined from the inelastic strains after the first half-cycle. The program was too costly in computing time to extend the cycling beyond $1\frac{1}{2}$ cycles.

The program was stopped and restarted 20 times for each case to change loads, temperatures, time increments, and material properties and to store the accumulated solution in case of a breakdown of the computer system. About 200 000 words of core memory on the Univac 1110 computer were required to run the problem. Each solution required approximately 5 to 7 hours of computing time.

LIFE PREDICTION - Cyclic lives to crack initiation were calculated by using Strainrange Partitioning when completely reversed inelastic strain cycles were obtained. For the unreversed strains (ratcheting), a linear-exhaustion-of-ductility concept should be used. In the present case, the only significant ratchet strains were creep strains induced during the 30-minute steady-state hold time. Therefore, the amount of damage due to creep ductility exhaustion was based on time fractions (time of stress to rupture at same stress) and the monotonic creep rupture data in (11). This method was simpler and probably more accurate than using ductility exhaustion based on the creep strain increment during the first cycle.

The Strainrange Partitioning relation presented in Fig. 5 for cast IN 100 alloy were used for the impingement-cooled blade. The cyclic stress-strain behavior shown in Fig. 6 and the Strainrange Partitioning relation in Fig. 7 for cast Mar M 302 alloy were used in the computations for the film-impingement-cooled vane. These data were obtained from cyclic tests of tubular specimens prepared from the same material billet as was used to fabricate the vanes. Data from tests conducted in a vacuum are reported in (13). Additional data obtained from tests conducted in air are also shown in Fig. 7; these show considerably lower lives than the data of (13) and were, therefore, used for the vane life prediction. In (2) it is demonstrated that the Strainrange Partitioning relations are relatively insensitive to temperature for materials whose ductility is not a strong function of temperature; however, such is not the case for Mar M 302. To make the Strainrange Partitioning relations presented in Fig. 7 usable,

they were corrected by the procedure described in (14). This procedure consists of multiplying the strain ranges by the ratio of the ductility at the temperature where inelastic straining initially occurred during the cycle to the ductility at the uniaxial specimen test temperature.

A problem arises in applying the one-dimensional stress analysis results for the film-impingement-cooled vane to life prediction at stress risers since the analysis only computes nominal stresses and strains. The nominal strain ranges have to be multiplied by strain concentration factors at nodes adjacent to discontinuities, such as the film-cooling slots and the inside wall in the leading-edge region where chordwise fins were present, as illustrated in Fig. 8. These strain concentration factors in the presence of inelastic strains were calculated by the Neuber method described in (15) that used $K_\epsilon = K_t^2/K_\sigma$, where K_ϵ is the strain concentration factor, K_t is the theoretical stress concentration factor and K_σ is the ratio of the actual to nominal stress range.

RESULTS AND DISCUSSION - IMPINGEMENT-COOLED BLADE

METAL TEMPERATURE GRADIENTS - The chordwise temperature distributions and the transient thermal responses at the leading and trailing edges are summarized in Figs. 9 and 10, respectively, for the four conditions that were considered: a design condition and three parametric variations.

Case 1 was the design condition. Temperatures at the leading edge were relatively low, as shown in Fig. 9(a); the hottest temperatures occurred in the trailing-edge region. The maximum chordwise temperature difference at midspan was about 111 K (200° F). During the acceleration and deceleration transients, the leading-edge temperature was lower than the average midspan temperature (Fig. 10(a)), indicating that the thermal stresses at the leading edge would always be tensile.

In case 2 the severity of the thermal loading was increased by increasing the steady-state temperature by an arbitrary amount of about 111 K (200° F) at the leading edge and decreasing it on the pressure side between the midchord and the leading edge, as shown in Fig. 9(b). This doubled the maximum chordwise temperature difference at midspan to about 222 K

(400° F). The transient response for case 2 was also made more severe by reducing the leading-edge temperature about 111 K (200° F) at the low-temperature part of the cycle. As a result of these changes, the leading-edge temperature curve in Fig. 10(b) crosses the average temperature curve, resulting in compressive thermal stresses at the steady-state condition and tensile thermal stresses at the beginning and end of the cycle.

A third condition (case 3) was analyzed with the same thermal load conditions as case 2 but with all the centrifugal and gas pressure loading removed. This changed the problem to one of a cantilevered vane. Since vanes are exposed to higher gas temperatures and, therefore, have to withstand higher metal temperatures than blades, a fourth condition (case 4) was considered in which all the metal temperatures were raised 56 K (100° F) from case 3. Figures 9(c) and 10(c) show the airfoil temperature distributions and transients for case 4. All centrifugal and gas pressure loads were also removed for case 4 to simulate a vane.

STRAIN CYCLES - The computed strain cycles for cases 1 to 4 at three airfoil locations are presented in Fig. 11. Locations A, B, and C were selected as generally the most critical locations in the leading-edge, trailing-edge, and pressure-side midchord regions, respectively. The most critical span position was usually at 30 percent of the span length as measured from the airfoil base. In these cycles, almost all the inelastic strain at the steady-state condition was due to creep, but plastic flow predominated in the transient parts of the cycle. The computations showed that the transient times were too short to induce significant creep strains.

There was no inelastic strain reversal in case 1. Since the leading-edge thermal stresses in case 1 were tensile, and therefore additive to the centrifugal stresses, the leading-edge location A in Fig. 11(a) exhibited tensile creep. In all four cases, location B was a hot spot and location C was a cold spot; therefore, the creep strains were always compressive at location B and always tensile at location C in cases 1 to 4. Compressive creep strains were not judged to be a danger to the structural integrity without inelastic strain reversal and were not considered in determining airfoil life, although they might eventually cause trailing-edge bowing in vanes.

When the leading-edge temperature was increased for cases 2 to 4, compressive creep occurred at location A. The only condition under which there was completely reversed inelastic straining was in case 2 where the compressive creep at location A was reversed by tensile plastic strain during deceleration (Fig. 11(b)). The largest tensile creep strains also occurred in case 2.

A comparison of Fig. 11(c) and (d) shows that the main effect of increasing the metal temperatures 56 K (100° F) was to cause a large increase in the plastic strain levels for the hot leading and trailing edges. Despite the higher temperatures, there was little change in the creep strain increments partly because of the lower yield stresses and, therefore, lower stress levels that resulted. However, the accuracies of the creep strain computations are problematic because of the extrapolation of the correlated creep characteristics to extremely small strains and time increments, as was discussed in the STRESS ANALYSIS section. For this reason the relaxed stresses at the end of the hold time were considered to be a more reliable basis on which to determine life than the ratcheted creep strain increments.

LIFE - Predicted cyclic lives for cases 1 to 4 are summarized in table 1(a). All the computed lives were determined from rupture due to tensile creep by time fractions, except for the leading edge in case 2, where Strainrange Partitioning was applied. In all four cases the most critical location was at or near location C in Fig. 11, which approximately coincided with the lowest temperature chordwise position in Fig. 9(b) to (d).

In case 1, the predicted blade life was 480 cycles at location C. The next most critical location was at the leading edge, where the life would be 640 cycles.

The only significant strain reversal occurred in case 2 at the leading edge. However, the predicted cyclic life based on the Strainrange Partitioning relation for the plastic tensile-compressive creep strain cycle is over 100 000 cycles for the inelastic strain range at location A (Fig. 11(b)). Thus, increasing the leading-edge temperature resulted in a huge improvement in leading-edge life for this configuration. This is in line with the temperature phasing benefits discussed in (14), which suggested that it might be beneficial to force the leading edge into compressive creep by

proper phasing of the temperatures at the edge and interior of the blade. The overall predicted improvement in blade life indicated in table 1(a) for case 2 (760 cycles as compared with 480 cycles for case 1) may be due to the reduction of about 17 K (30° F) in the average steady-state temperature shown by comparing Figs. 10(a) and (b). Increasing the severity of the temperature gradient and transient response did not appear to deleteriously affect the blade life. These predictions are in qualitative agreement with results of cyclic tests of impingement-cooled airfoil specimens in the thermal fatigue facility described in (16). These tests disclosed that a thin-wall, hollow airfoil with no stress concentrations, no webs to act as heat sinks, and no steady-state hold time was almost immune to low-cycle fatigue failure even with leading-edge temperatures as high as 1311 K (1900° F) and chordwise temperature gradients as high as 556 K (1000° F).

The predicted results for cases 3 and 4 are what would be intuitively expected. Removing the blade mechanical loads and reducing the problem to that of a cantilevered vane in case 3 resulted in a substantial improvement in the airfoil life. Increasing the temperature levels by 56 K (100° F) in case 4 resulted in a reduction in life from 2200 cycles for case 3 to 1000 cycles for case 4.

RESULTS AND DISCUSSION - FILM-IMPINGEMENT-COOLED VANE

METAL TEMPERATURE GRADIENTS - Transient temperature distributions shown in Fig. 12 were obtained from experimental data and theoretical heat transfer analyses for cycles over an effective gas temperature range of 922 to 1644 K (1200° to 2500° F) with a coolant temperature of 811 K (1000° F). The vane hot spots were at the upstream sides of the pressure and suction surface film-cooling slots (locations B and C). The leading-edge stagnation point was hotter than the bulk temperature of the vane during the acceleration part of the cycle and colder during deceleration. The inside wall at location A in the leading-edge region was the cold spot during most of the deceleration.

STRAIN CYCLES - The computed nominal inelastic-strain versus temperature loops at the most critical locations are shown in Fig. 13 for the fifth cycle. The inelastic strains were predominately plastic since the transient times

were very short and the cycles did not include any steady-state hold times. These loops were obtained from the nominal total strain cycles presented in (4) by subtracting the elastic strain components.

The vane airfoil was modeled for the stress analysis with four layers of elements across the wall. Location A in the leading-edge region was at the inmost element and adjacent to the chordwise fins. The fins could not be considered in the one-dimensional stress analysis and, therefore, the computed inelastic strain range for location A was multiplied by a strain concentration factor for life prediction. Location B' in Fig. 13 was on the downstream side of the pressure-surface, film-cooling slot and should not be confused with location B in Fig. 12, which is a hot spot on the upstream side. The nominal inelastic strain range for location B' in Fig. 13 did not take into account the discontinuity due to the adjacent film-cooling slot and, therefore, was also multiplied by a strain concentration factor. By Neuber methods (15), the strain concentration factors were calculated as 3.91 for the chordwise fins at location A and 5.59 for the corners of the film-cooling slots at location B'.

LIFE - The predicted lives presented in table 1(b) were obtained from the Strainrange Partitioning relation shown in Fig. 7 for tensile plasticity reversed by compressive plasticity for the vane alloy Mar M 302 in an air environment. Since the ductility of this material is influenced by temperature in a known manner, the inelastic strain ranges presented in Fig. 7 as a function of cyclic life were corrected, according to the effect of temperature on ductility, by using the method of (14). A factor of 0.477 for location A and a factor of 0.293 for location B' were applied to the strain ranges. These correction factors were based on the ratio of the ductilities at the temperatures where tensile inelastic straining initially occurred (1033 K (1400° F) at location A and 839 K (1050° F) at location B') to the ductility at the test temperature of 1273 K (1832° F).

The predicted life for complete fracture of 60 cycles at location A is somewhat greater than the crack initiation life indicated by the experimental evidence. At the end of 60 cycles (20 at the analytical condition and 40 at less-severe conditions) one of the test vanes was sectioned for inspection of the inside surface at the leading edge. This inspection revealed

cracking at the base of many of the chordwise fins (location A), as shown by the photomicrographs of Fig. 14. The wide crack seen in Fig. 14(a) almost propagated to the outside surface; other signs of crack initiation are visible in Fig. 14(b). The greater predicted life for location A may be due to the fact that the Mar M 302 test specimens used to obtain the data in Fig. 7 were cast smooth, machined, and polished; the internal surfaces of the vane would have much rougher surfaces and, therefore, lower lives.

The predicted life of eight cycles at location B' is consistent with the experimental results, although the exact number of cycles at which failure began is unknown. Fatigue cracks were found on the downstream side of the pressure-surface, film-cooling slots after the 60 cycles of testing. Similar cracks were found in 69 out of 72 vanes of this configuration (Fig. 15), many of which had undergone less than 40 cycles in a research turbojet engine operating at essentially the same conditions. The leading-edge crack shown in Fig. 15 was revealed by metallographic inspection to have initiated at the inside surface and propagated through the wall.

The severity of the fatigue problem for the film-impingement-cooled airfoil configuration was caused by the presence of the web, which remained cold during acceleration and hot during deceleration and constrained the movement of the airfoil walls. Even if the effects of the stress risers were neglected, the inelastic strain ranges for locations B' and A were large enough that failures would have been predicted in 53 and 270 cycles, respectively. The thermal gradients and levels shown for the film-impingement-cooled vane in Fig. 12 appear to be no more severe than those shown in Figs. 9(c) and 10(c) for case 4 of the impingement-cooled airfoil.

SUMMARY OF RESULTS

The inelastic strain cycles and the cyclic lives to crack initiation of an impingement-cooled blade under various thermal and mechanical loads and of a film-impingement-cooled vane were calculated from cyclic stress analysis programs, using computed transient metal temperatures and either a Strainrange Partitioning or time fractions approach, where each was applicable. The results of these analytical studies

can be summarized as follows:

1. The life predictions made by using Strainrange Partitioning and time fraction methods were generally consistent with, although not completely verified by, limited experimental evidence from cyclic tests in research cascade facilities of the same or similar cooling configurations.

2. The Strainrange Partitioning approach appears to be applicable to a constrained airfoil construction, such as in the film-impingement-cooled vane. In a constrained airfoil it is relatively easy to induce large inelastic strains and strain reversal during the transient parts of the cycle.

3. Time fractions were more applicable for life prediction with the fully impingement-cooled blade than Strainrange Partitioning. In a thin-wall, hollow airfoil construction with no webs, such as exists in the impingement-cooled blade, it is difficult to induce inelastic strain reversal even under severe thermal transients. The damage due to inelastic strain hysteresis was of minor consequence compared with the monotonic creep ratcheting damage.

4. Increasing the severity of the thermal transients and gradients for the impingement-cooled blade did not deleteriously affect the predicted lives. Raising the leading-edge temperature above the average span-section temperature actually increased the predicted life of the leading edge by putting it in compression.

5. As expected, removing the airfoil mechanical loads to simulate a vane while maintaining the same thermal loads increased the predicted life. However, changing the thermal loads by increasing the metal temperature levels 56 K (100° F) resulted in a reduction in predicted airfoil life of about 50 percent.

APPENDIX - PLASTICITY-CREEP STRESS AND STRAIN EQUATIONS

Effective stress is represented by

$$\bar{\sigma} = \sqrt{\frac{3}{2} S_{ij} S_{ij}} \qquad \text{(A1)}$$

and the effective plastic strain increment is represented by

$$d\bar{\epsilon}^{p} = \sqrt{\frac{2}{3} d\epsilon^{p}_{ij} \, d\epsilon^{p}_{ij}} \qquad \text{(A2)}$$

where $d\bar{\epsilon}^p_{ij}$ is the incremental plastic strain vector and S_{ij} is the stress-deviation tensor. The components of S_{ij} are

$$S_x = \sigma_x - \frac{(\sigma_x + \sigma_y + \sigma_z)}{3} \tag{A3}$$

$$S_y = \sigma_y - \frac{(\sigma_x + \sigma_y + \sigma_z)}{3} \tag{A4}$$

$$S_z = \sigma_z - \frac{(\sigma_x + \sigma_y + \sigma_z)}{3} \tag{A5}$$

where σ_x, σ_y, and σ_z denote the normal stress components in the directions of the global axes and

$$S_{xy} = \tau_{xy} \tag{A6}$$

$$S_{xz} = \tau_{xz} \tag{A7}$$

$$S_{yz} = \tau_{yz} \tag{A8}$$

with τ_{xy}, τ_{xz}, and τ_{zy} denoting the shear components.

The uniaxial secondary creep rate is expressed in exponential form

$$\dot{\epsilon}^c = A\sigma^n \tag{A9}$$

where A is a constant and n is a function of temperature.

The multiaxial secondary creep rate is

$$\dot{\epsilon}^c_{ij} = \frac{3}{2} A\bar{\sigma}^{n-1} S_{ij} \tag{A10}$$

At the end of time t the creep strain is

$$\epsilon^c_{ij} = \frac{\sigma_{ij}}{E^K_{ij}} \left[1 - \bar{\epsilon}^{(E^K_{ij}/\eta^K_{ij})t} \right] + \dot{\epsilon}^c_{ij} t \tag{A11}$$

Kaufman

where σ_{ij} and ϵ_{ij} are the stress and creep

strain vectors and E^K_{ij} and η^K_{ij} are the Kelvin model spring and dashpot constants, respectively.

The effective incremental creep strain is given by

$$d\bar{\epsilon}^c = \sqrt{\frac{2}{3} d\epsilon^c_{ij} \, d\epsilon^c_{ij}} \qquad (A12)$$

which is analogous to equation (A2) for the incremental plastic strain.

REFERENCES

1. S.S. Manson, G. R. Halford, and M. H. Hirschberg, ''First National Pressure Vessel and Piping Conference on Design for Elevated Temperature Environment.'' D. H. Pai, ed., New York: Am. Soc. Mech. Engrs., 1971, pp. 12-24.

2. G. R. Halford, M. H. Hirschberg, and S. S. Manson, ''Symposium on Fatigue at Elevated Temperatures.'' STP-520, Philadelphia,: Am. Soc. Testing Mater., 1972, pp. 658-669.

3. G. R. Halford and S. S. Manson, ''Life Prediction of Thermal-Mechanical Fatigue Using Strainrange Partitioning.'' NASA TM X-71829, 1975.

4. A. Kaufman, D. J. Gauntner, and J. W. Gauntner, ''Cyclic Stress Analysis of an Air-Cooled Turbine Vane.'' NASA TM X-3256, 1975.

5. A. Kaufman, ''Analytical Study of Cooled Turbine Blades Considering Combined Steady-State and Transient Conditions.'' NASA TM X-1951, 1970.

6. B. A. Boley and J. H. Weiner, ''Theory of Thermal Stresses.'' Ch. 10, New York: John Wiley & Sons, Inc., 1960, pp. 307-355.

7. S. Utku, M. S. M. Rao, and G. J. Dvorak, ''ELAS 65 Computer Program for Equilibrium Problems of Elastic-Thermoplastic Solids and Structures.'' Structural Mechanics Ser. 15, Duke Univ. (also AROD-9570-2-E; AD-775536), Nov. 1973.

8. S. Utku, J. Q. Tarn, and G. J. Dvorak, ''ELAS 55 Computer Program for Equilibrium Problems of Thermo-Viscoelastic-Plastic Solids and Structures.'' Structural Mechanics Ser. 21, Duke Univ., Sept. 1974.

9. R. E. Gaugler, ''TACT1, A Computer Program for the Transient Thermal Analysis of a Cooled Turbine Blade or Vane Equipped with a Coolant Insert.'' To be published.

10. B. Hunsaker, Jr., D. K. Vaughan, and J. A. Stricklin, ''A Comparison of the Capability of Four Hardening Rules to Predict a Material's Plastic Behavior.'' Rpt. 75-51, Texas A&M Univ., June 1975.

11. ''Engineering Properties of IN 100 Alloy.'' International Nickel Co., 1968.

12. M. H. Hirschberg, ''Manual on Low Cycle Fatigue Testing Facility.'' STP-465, New York: Soc. Testing Mater. 1970.

13. K. D. Sheffler, ''The Partitioned Strainrange Fatigue Behavior of Coated and Uncoated Mar-M-302 at 1000° C (1832° F) in Ultrahigh Vacuum.'' TRW ER-7723, TRW Mater. Tech. Lab., June 1974; also NASA CR-134626.

14. S. S. Manson, ''Symposium on Fatigue at Elevated Temperatures.'' STP-520, Philadelphia, PA: Am. Soc. Testing Mater., 1972, pp. 744-782.

15. R. W. Landgraf and F. D. Richards, ''Fatigue Life Predictions for a Notched Member under Complex Load Histories.'' Paper 750040 presented at SAE Automotive Engineering Congress, Detroit, Feb. 1975.

16. J. N. B. Livingood, H. H. Ellerbrock, and A. Kaufman, ''NASA Turbine Cooling Status Report.'' NASA TM X-2384, 1971.

Table 1. - Predicted Cyclic Lives

(a) Impingement-cooled blade

Case	Leading-edge location A	Pressure-surface location C	Other critical locations
	Number of cycles to failure		
1	640	480	---
2	[b]>100 000	1700	[a]760
3	-------	2200	---
4	-------	1000	---

(b) Film-impingement-cooled vane

	Leading-edge location A	Pressure-side location B'
	Number of cycles to failure	
	[c]60	[c]8

[a]Pressure surface adjacent to location C. Locations A and C are at 30 percent of span and are shown in Fig. 11.
[b]Strainrange Partitioning used. Other lives were based on time fraction due to creep.
[c]Strainrange Partitioning used. Locations A and B are shown in Fig. 13.

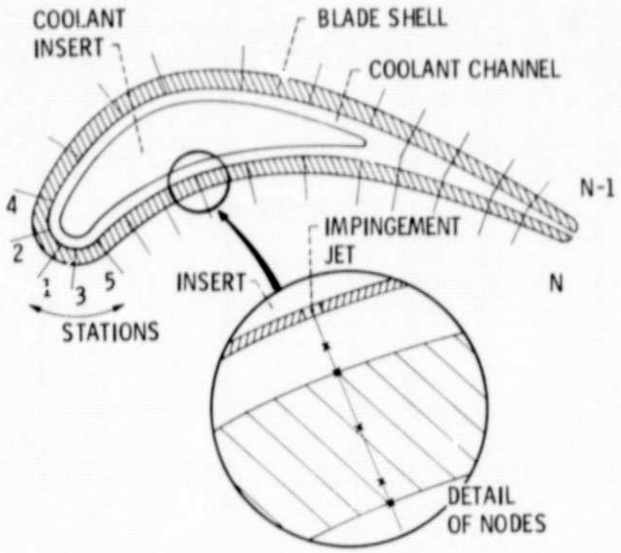

Figure 1. - Cross section of impingement-cooled blade.

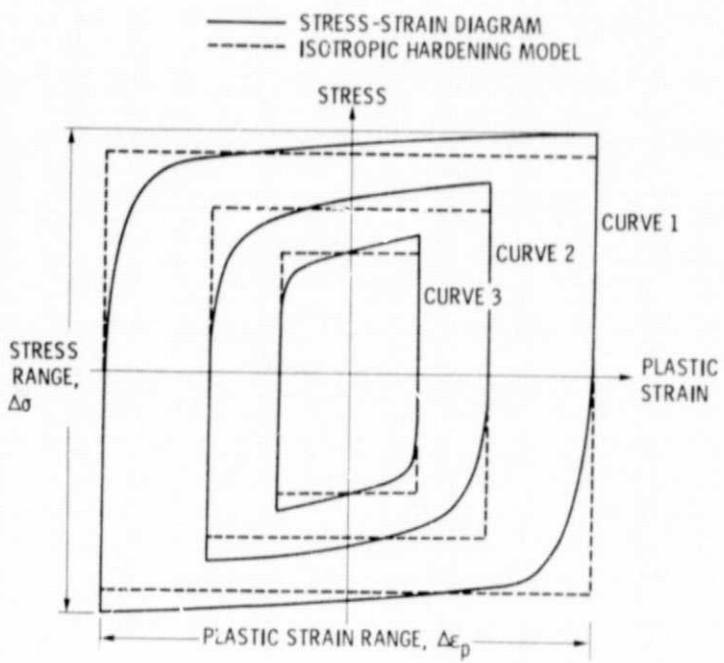

Figure 2. - Cyclic stress-strain behavior.

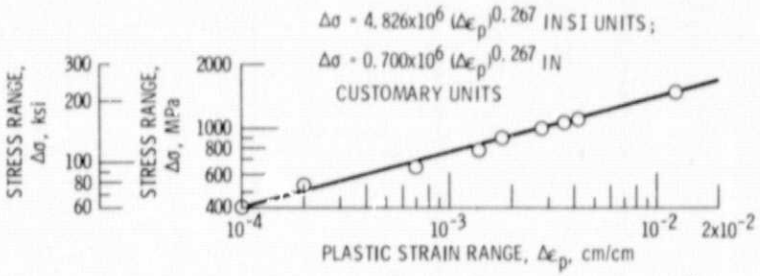

Figure 3. - Cyclic stress-strain behavior of cast IN 100 at 1200 K (1700° F). Frequency, 0.5 Hz; $\Delta W_p = 0.5785\ \Delta\sigma\ \Delta\epsilon_p$.

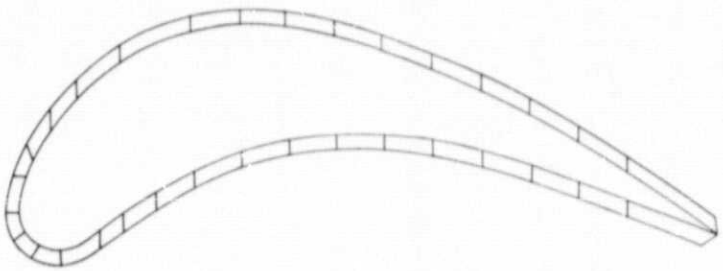

Figure 4. - Finite-element modeling of airfoil cross section for impingement-cooled blade. Airfoil chord length, 3.81 cm (1.50 in.); airfoil span length, 3.81 cm (1.50 in.).

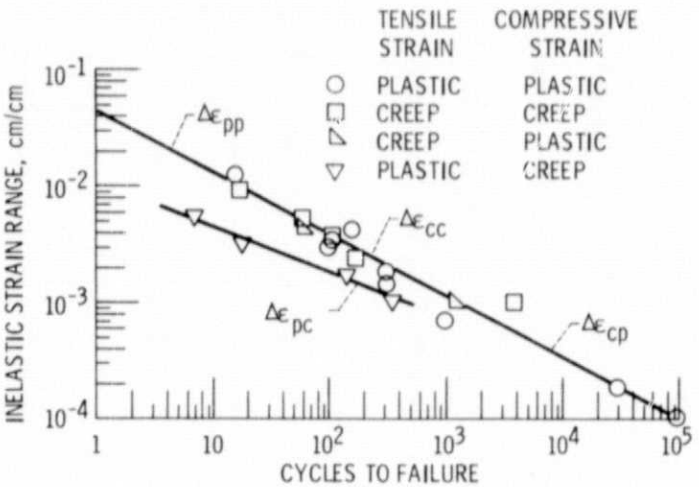

Figure 5. - Partitioned strain range versus life relations for cast IN 100 alloy at 1200 K (1700° F). Frequency, 0.65 Hz. (NASA Lewis data by G. R. Halford.)

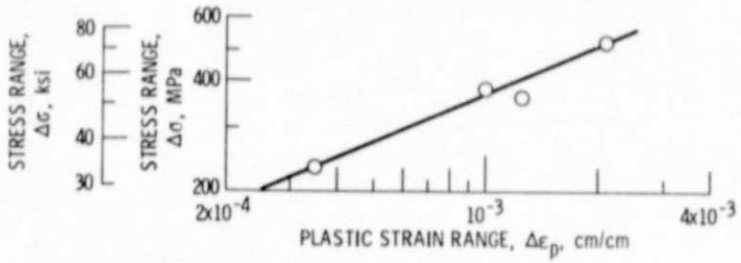

Figure 6. - Cyclic stress-strain behavior of Mar M 302 at 1273 K (1832° F). (From ref. 13.)

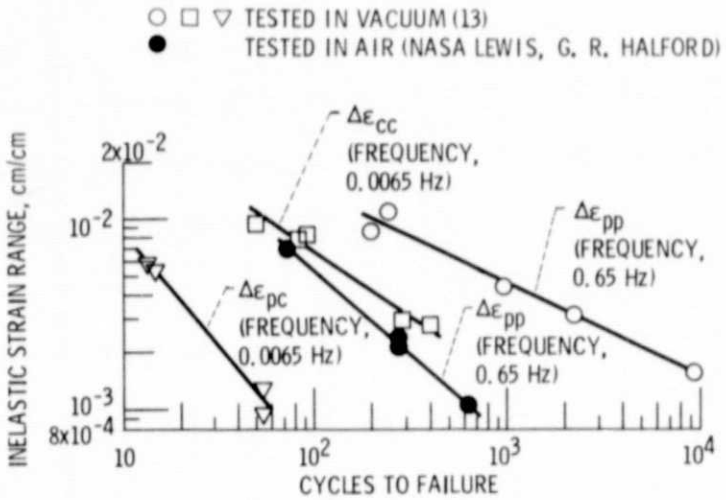

Figure 7. - Partitioned strain range versus life relations for Mar M 302 alloy at 1273 K (1832° F).

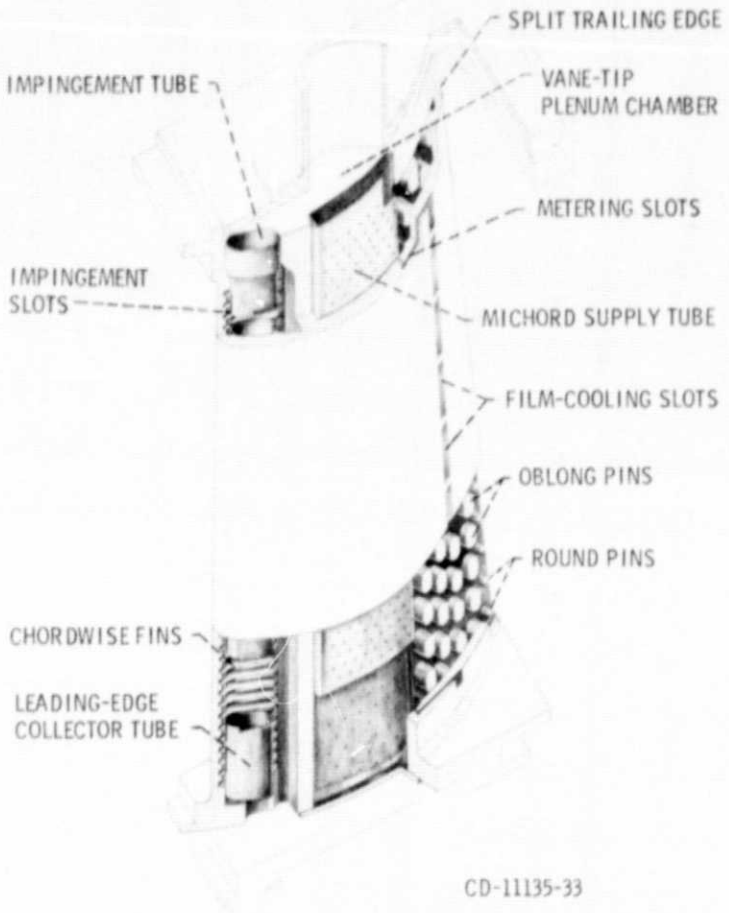

Figure 8. - Film-impingement-cooled vane.

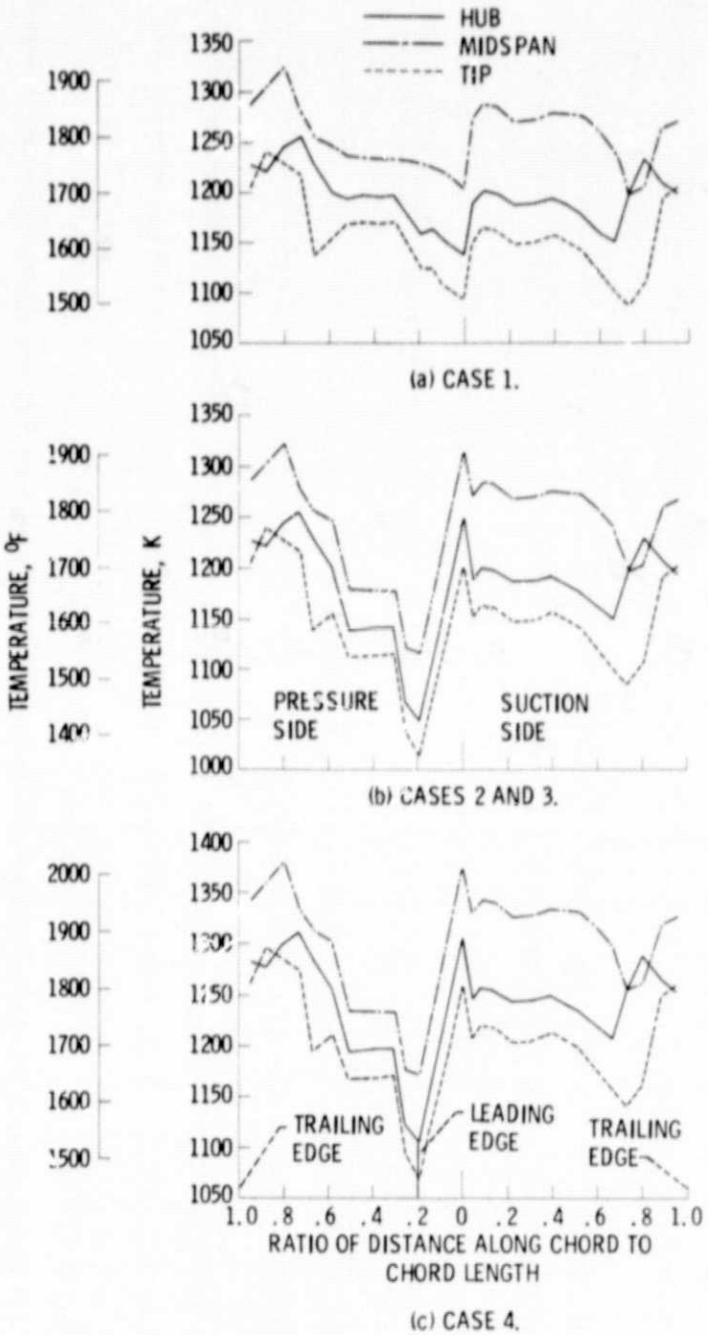

Figure 9. - Chordwise temperature distribution at high-gas-temperature, steady-state condition for impingement-cooled blade.

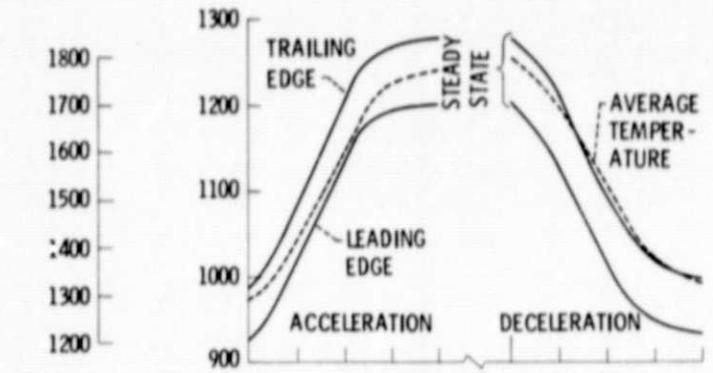

(a) CASE 1.

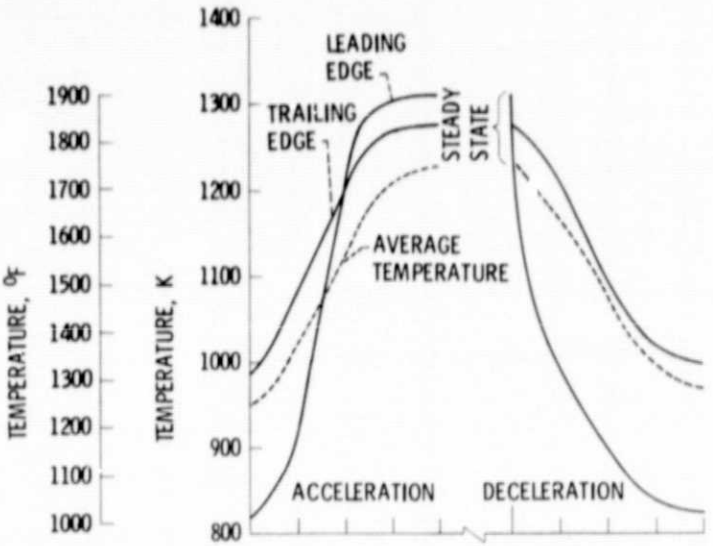

(b) CASES 2 AND 3.

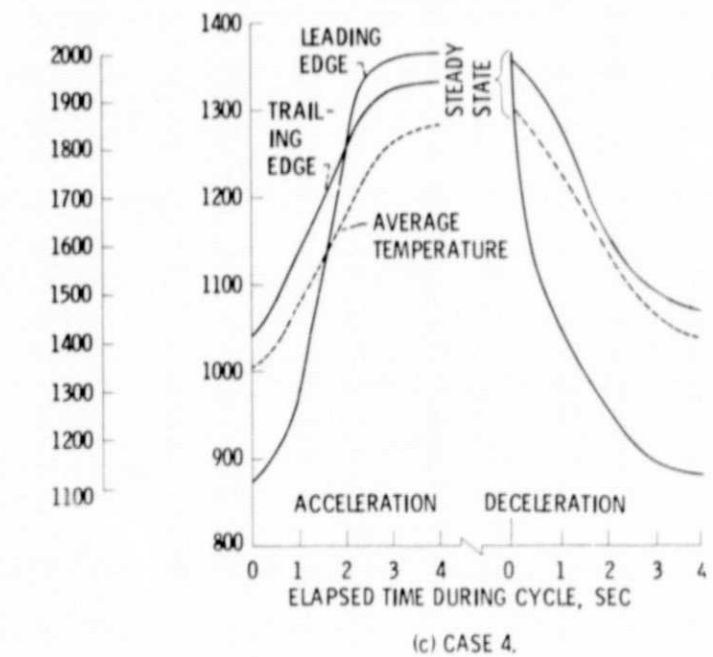

(c) CASE 4.

Figure 10. - Metal temperature cycle at midspan for impingement-cooled blade.

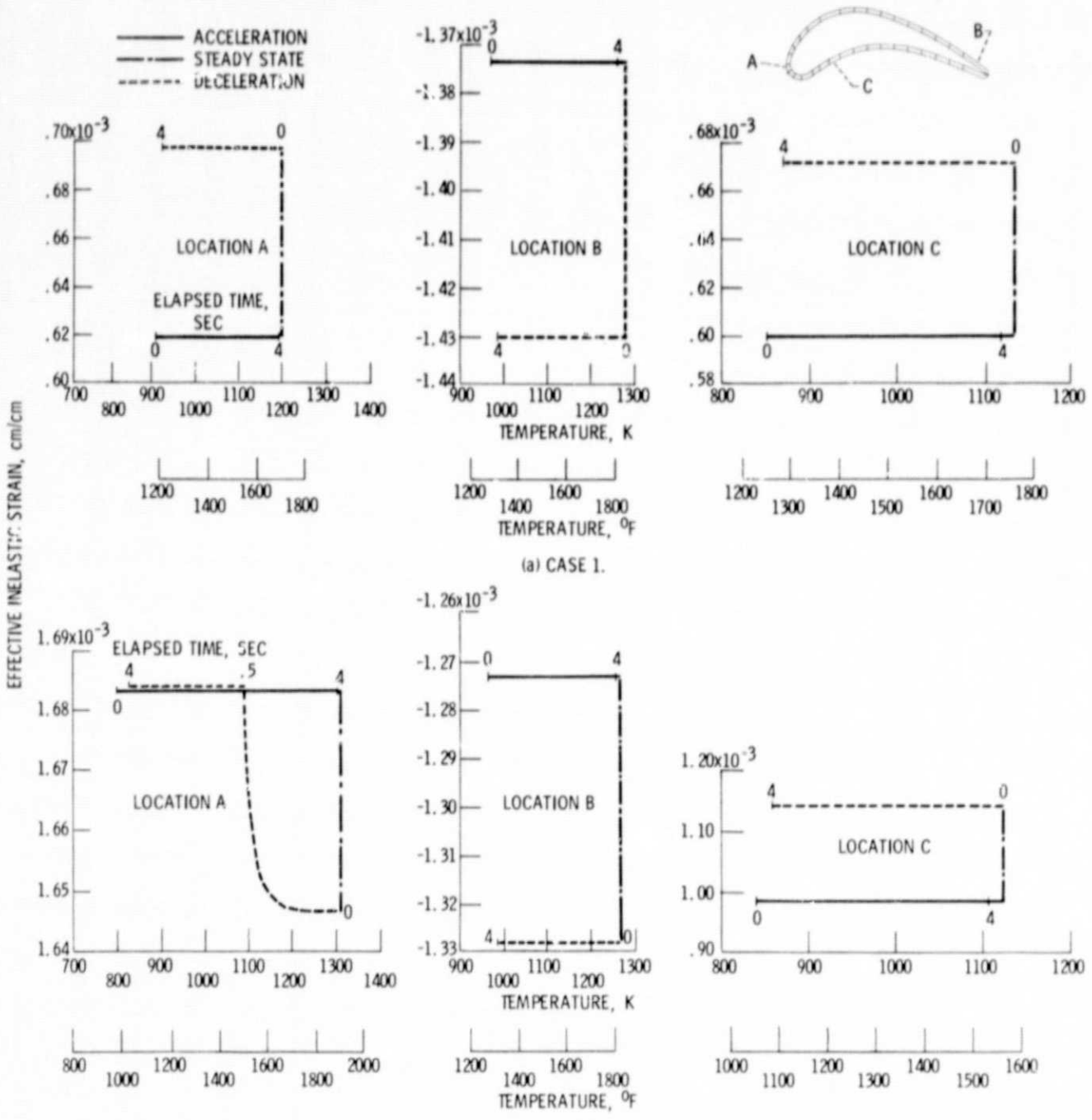

Figure 11. - Strain-temperature cycles for impingement-cooled blade.

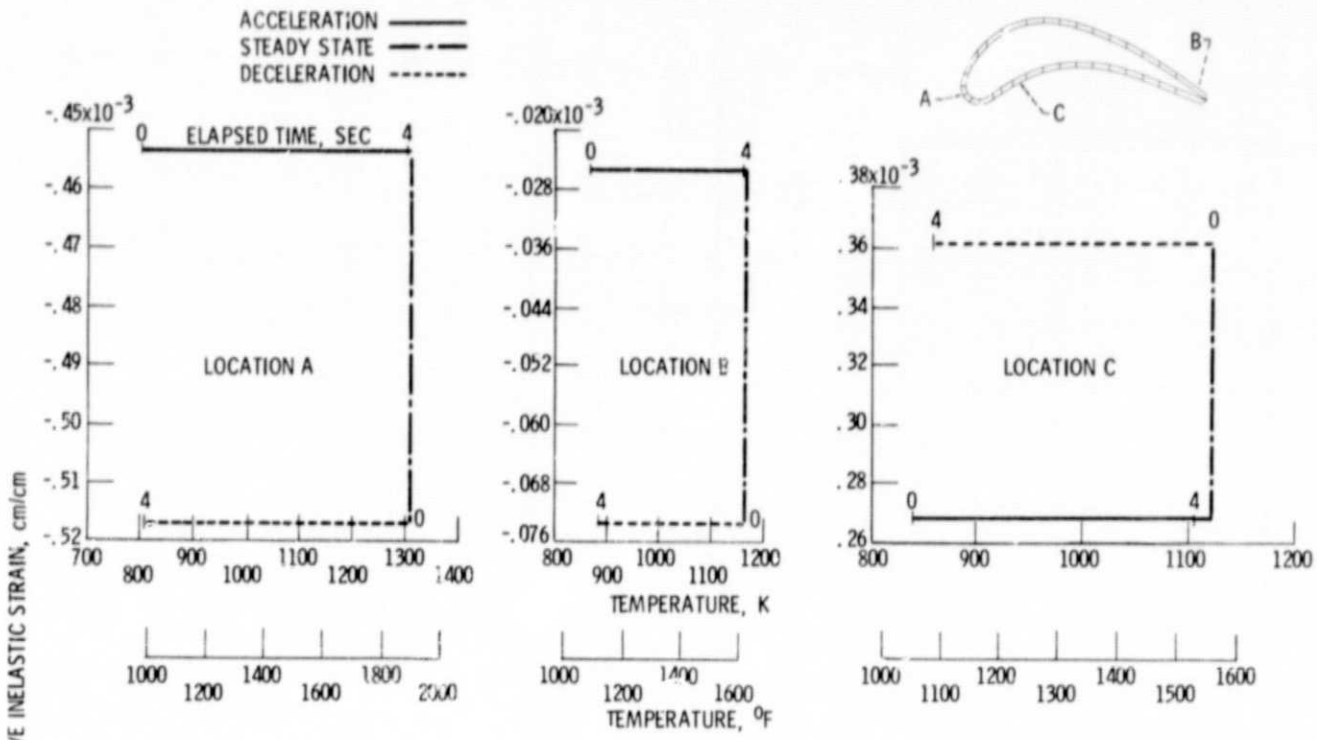

(c) CASE 3.

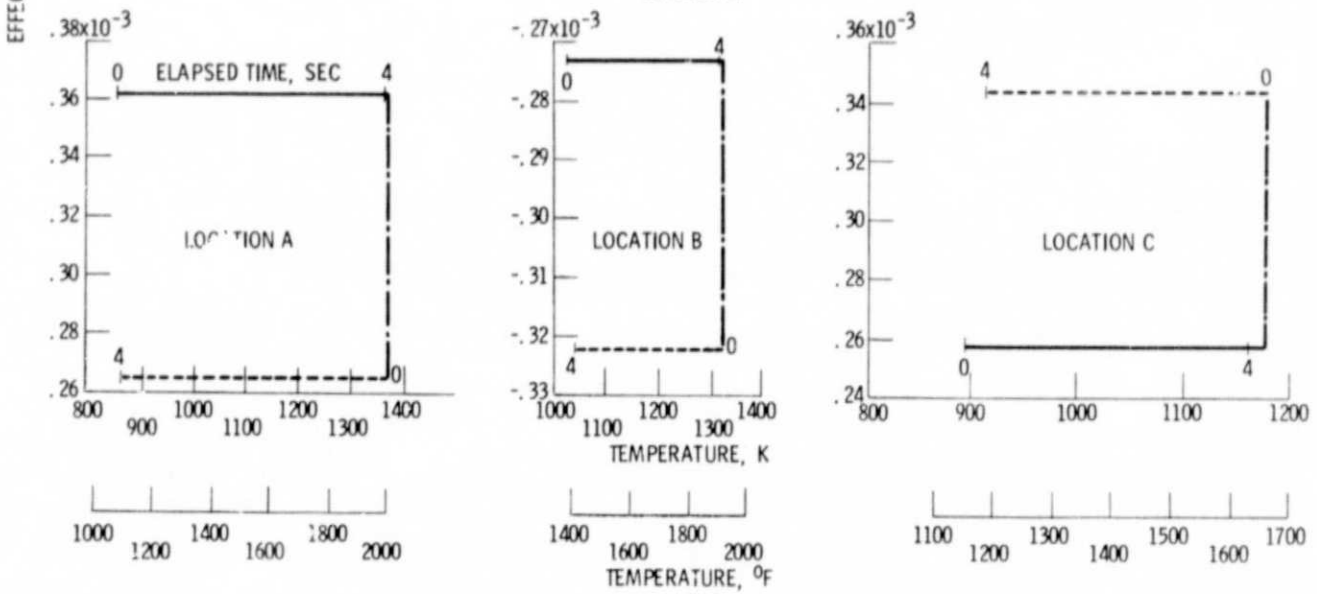

(d) CASE 4.

Figure 11. - Concluded.

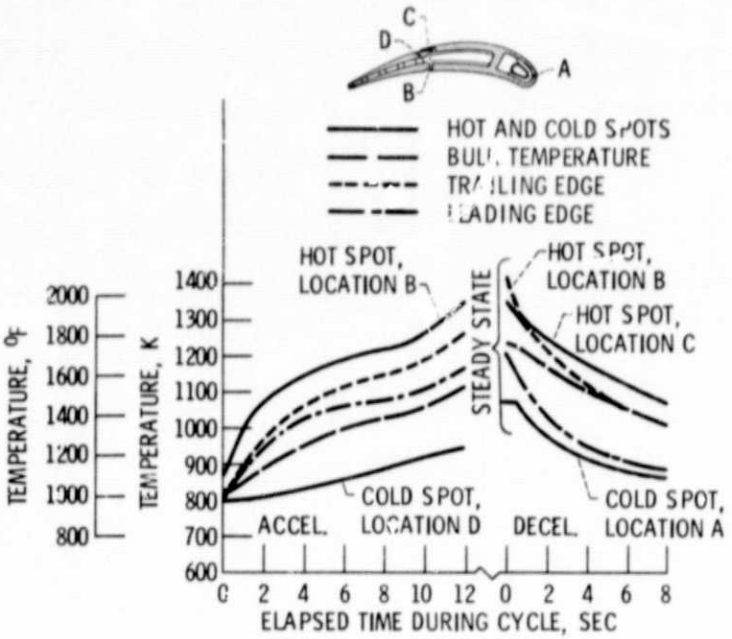

Figure 12. - Metal temperature cycle at midspan for film-impingement-cooled vane.

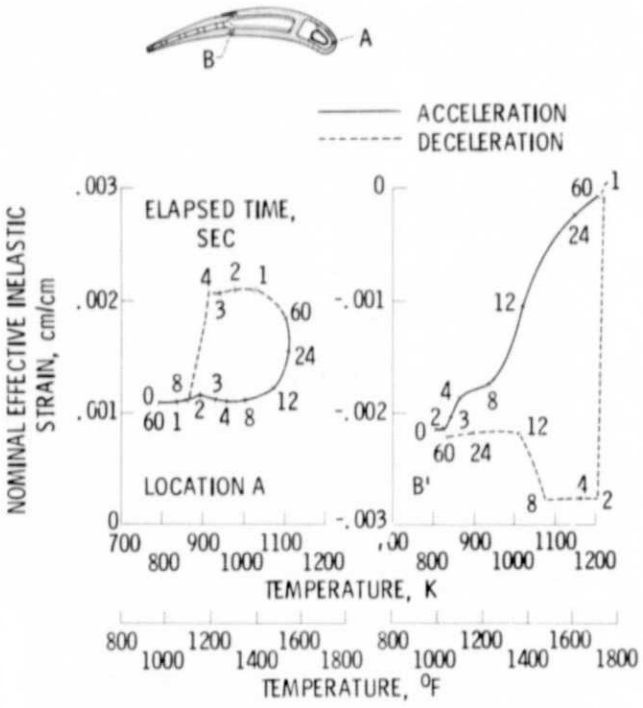

Figure 13. - Strain-temperature loops for film-impingement-cooled vane.

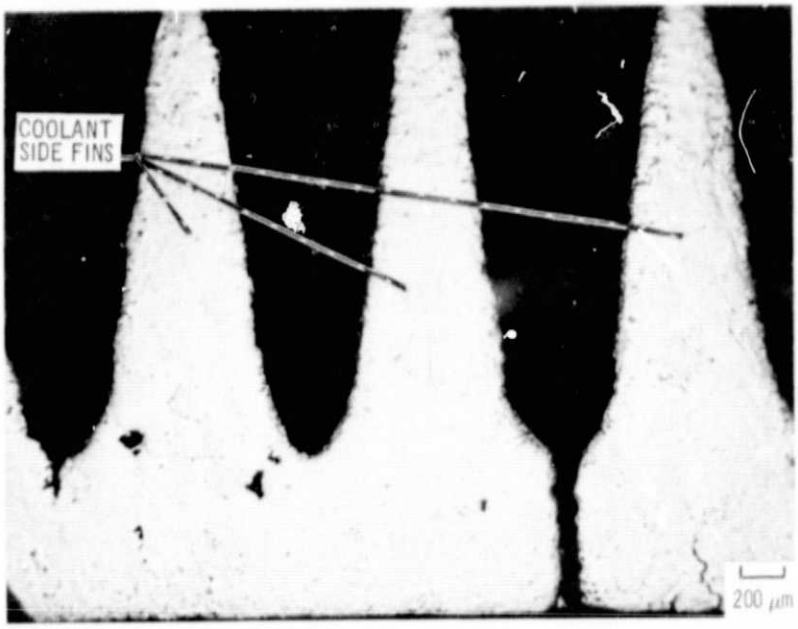

(a) CRACK PROPAGATION THROUGH AIRFOIL WALL.

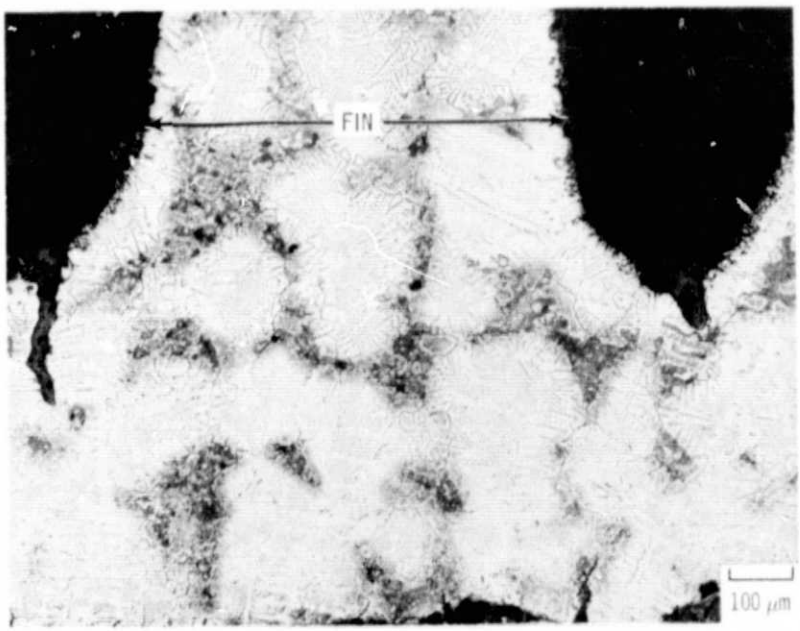

(b) CRACK INITIATION AT BASE OF FINS.

Figure 14. - Fatigue cracks at inside surface of leading edge of film-impingement-cooled vane.

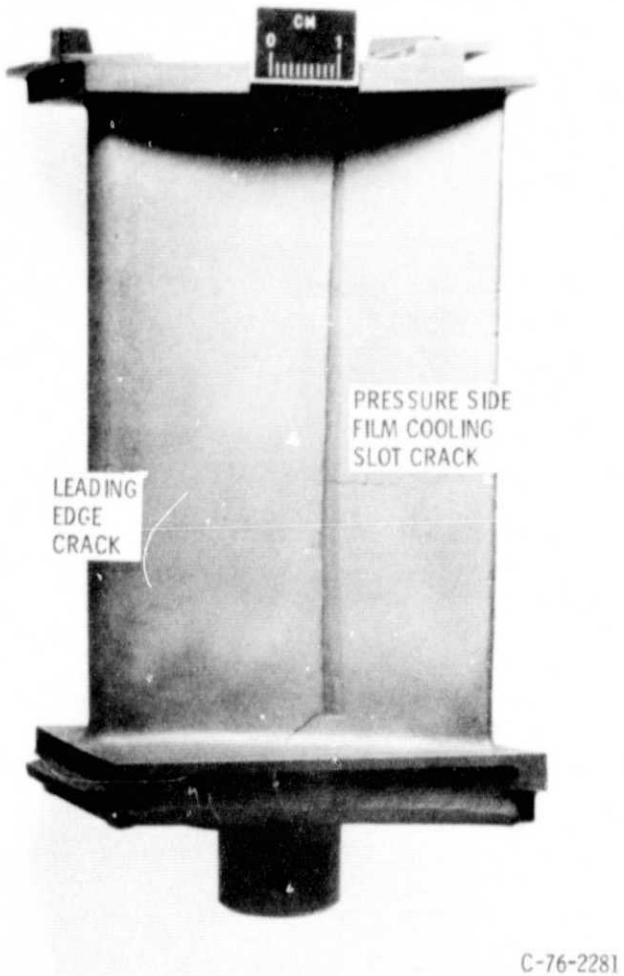

Figure 15. - Fatigue cracks in film-impingement-cooled vane.